Supporting Information

Cejas *et al.* 10.1073/pnas.0800291105

SI Text

Peptides. ***Synthesis.*** Fmoc-amino acids, 1-hydroxybenzotriazole; 2-[(1*H*-benzo-triazol-1-yl)-1,1,3,3-tetramethyluronium hexafluorophosphate; $(i\text{-Pr})_2$NEt, *N*-methylpyrrolidin-2-one, and CH_2Cl_2 were purchased from Applied Biosystems. Piperidine was purchased from Sigma–Aldrich. Fmoc-Gly-Wang and Fmoc-Phe-Wang resins were purchased from Bachem and Novabiochem (Merck), respectively.

Purification. Peptide purification was performed by RP-HPLC on a Gilson instrument (two 306 pumps, 819 injection valve, 215 liquid handler) equipped for column heating (water-filled circulator compartment; PolyScience 1166 circulation heater) at 60°C (Zorbax 300 SB-C18 column: 7 μm, 21.2 x 150 mm) with a linear gradient of 5–95% B added to A (A: 0.05% CF_3CO_2H and water; B: 0.05% CF_3CO_2H and MeCN) over 15 min (flow rate: 20 ml/min; UV detection at 210 nm). Fractions were analyzed by LC/MS on an Agilent 1100 instrument coupled to an Agilent MSD Mass Spectrometer at 60°C (Zorbax 300SB-C18 column: 3.5 μm, 15 cm $\times$ 2.0 mm) with a linear gradient of 10–40% B added to **A** (**A**: 0.1% HCO_2H, 0.01% CF_3CO_2H, and water; **B**: 0.1% formic acid, 0.01% CF_3CO_2H, and MeCN) over 23 min (flow rate: 0.4 ml/min; retention times: **1a**, 12.7 min; **1b**, 10.7 min; **1c**, 9.5 min; **1d**, 6.2 min; **2**, 13.1 min). For each peptide, fractions containing the desired material were combined and lyophilized to yield white powders. HPLC analysis indicated that each peptide was ≈85% pure, with ≈10% of the corresponding peptide missing one Pro residue. Peptide content was determined by amino acid analysis.

Peptides **1a–d** were purified further with the Agilent 1100 LC-MS system at 65°C (Zorbax 300 SB-C18 column: 7 μm, 21.2 x 150 mm) with linear gradients of acetonitrile/water with 0.1% CF_3CO_2H (flow rate: 30 ml/min). The MS detector was programmed in the ESI^+/SIM mode to monitor molecular ions for the peptide of interest. Molecular ions selected as target masses to trigger fraction collection were (peptide, *m*/*z*, gradient conditions): **1a**, 1025, 15–20% MeCN/15 min; **1b**, 1493.5, 10–20% MeCN/20 min; **1c**, 984, 10–20% MeCN/20 min; **1d**, 935.8, 1–20% MeCN/20 min. Peptides were isolated by vacuum evaporation and then freeze-drying. For these refined samples of **1a–d**, molecular weights were confirmed by MALDI-TOF MS (Applied Biosystems Q-Star Elite Q-Tof system, orthogonal MALDI source, Nd-YAG laser). Purities (see main text) were determined by analytical RP-HPLC at 65°C (Agilent 1100 instrument; Zorbax 300 SB-C18 column: 3.5 μm, 150 $\times$ 4.6 mm; linear gradient of 5–25% MeCN in water plus 0.1% CF_3CO_2H over 35 min; flow rate: 1 ml/min; UV detection: 210 nm); retention times were: **1a**, 25.3 min; **1b**, 22.7 min; **1c**, 21.8 min; **1d**, 14.3 min.

Computational Work. Because the computed energies are gas-phase enthalpies (ΔH), one cannot determine the entropic or desolvation contributions, which would probably be similar for each homodimer. Assuming that the binding free energy (ΔG) for $(\mathbf{1a}')_3/(\mathbf{1a}')_3$ would be unlikely to exceed −18 kcal/mol, the non-enthalpic contribution (ΔS) could amount to nearly +60 kcal/mol. This non-enthalpic energy component may explain why 32-mers **1a** and **1b** self-associate well into biofunctional fibrils, whereas **1c** and **1d** do not, according to the AFM results. Subdivision of the total binding energy into coulombic and dispersive terms revealed some interesting patterns. The dispersive contributions for homodimers $(\mathbf{1a}')_3/(\mathbf{1a}')_3$ and $(\mathbf{1b}')_3/(\mathbf{1b}')_3$ would be expected to be similar since there is comparable steric bulk from contacts across the junction (despite differing group orientations), and the substantial loss of coulombic energy is expected in going from a fluorobenzene/benzene to a benzene/benzene interaction. However, there was surprisingly little loss of coulombic energy on replacing benzyl by *i*-Bu, in going from $(\mathbf{1b}')_3/(\mathbf{1b}')_3$ to $(\mathbf{1c}')_3/(\mathbf{1c}')_3$, despite the diminished electrostatic character of Leu. The dramatic loss of dispersive energy in going from $(\mathbf{1b}')_3/(\mathbf{1b}')_3$ to $(\mathbf{1c}')_3/(\mathbf{1c}')_3$ was expected, because dispersion is inversely related to r^6 (r = interatomic distance) and the aryl/aryl atoms can get closer together than the aryl/alkyl atoms. Homodimer $(\mathbf{1d}')_3/(\mathbf{1d}')_3$ has few opportunities for dispersive energy gain, given the absence of the hydrophobic terminal groups. However, the coulombic energy for $(\mathbf{1d}')_3/(\mathbf{1d}')_3$ was increased over $(\mathbf{1c}')_3/(\mathbf{1c}')_3$ because of the absence of steric bulk and a small collapse of the head-to-tail junction in $(\mathbf{1d}')_3/(\mathbf{1d}')_3$. The coulombic network at the junctions is extremely complex, involving both attractions and repulsions across the ion pairs and peptide bonds. The major H-bonds can convey the coulombic energy trends. Homodimer $(\mathbf{1d}')_3/(\mathbf{1d}')_3$ (5 H-bonds) has two stronger H-bonds than $(\mathbf{1b}')_3/(\mathbf{1b}')_3$ and $(\mathbf{1c}')_3/(\mathbf{1c}')_3$ (3 H-bonds), but it has the same pattern of H-bonds as $(\mathbf{1a}')_3/(\mathbf{1a}')_3$ (5 H-bonds). Thus, $(\mathbf{1a}')_3/(\mathbf{1a}')_3$ has the most stable junction without any serious perturbations of the favorable H-bond network.

AFM Background. AFM is a powerful tool for characterizing biological assemblies and macromolecules (1, 2). It can provide spatial information along and perpendicular to the surface of a deposited film with resolution on the order of 1 nm. A common AFM imaging mode for macromolecules is the intermittent contact mode, also known as AC Mode or Tapping Mode (3). In these modes, the cantilever is oscillated at its resonance frequency with a free amplitude, A_0. While the cantilever approaches the surface, the oscillating amplitude is reduced to a value A, which depends on the distance to the surface. The ratio $r = A/A_0$ defines the damping of the amplitude while the tip is in contact with the surface and is proportional to the applied force. By keeping damping of the amplitude constant, the surface topography can be mapped. A phase image can be recorded simultaneously with the surface topography. In this image, the phase shift between the free oscillation in air and the oscillation while the tip is in contact with the surface is recorded (4). Since the phase shift depends as much on the sample's viscoelastic properties as on the adhesive potential between the sample and tip, the phase image serves to outline domains of varying material contrast, without describing the nature of the material properties (5–9).

Platelet Studies. Platelet-rich plasma (PRP) concentrate from healthy human volunteers was purchased from Biological Specialties. The PRP was not older than 5 h, since PRP that was 24-h old gave attenuated responses to collagen. The PRP was centrifuged at 730 $\times$ *g* for 15 min and the resulting platelet pellet was washed twice in CGS buffer [13 mM sodium citrate, 30 mM glucose, and 120 mM NaCl (pH 6.5)] containing 1 U/ml apyrase (grade V, Sigma–Aldrich) and resuspended in Tyrode's buffer [140 mM NaCl, 2.7 mM KCl, 12 mM $NaHCO_3$, 0.76 mM Na_2HPO_4, 5.5 mM dextrose, 5.0 mM Hepes, and 0.2% BSA (pH 7.4)]. The "washed" platelets were diluted to 3×10^8 platelets/ml and kept for >45 min at 37°C before use. For the assay, 105 μl of washed platelets, 2 mM $CaCl_2$, and 2.5 mM of fibrinogen were added to a 96-well microtiter plate.

Platelet aggregation induced by collagen or **1a** was inhibited

by the GP IIb/IIIa antagonist RWJ-53308 (10) with an IC_{50} of 200–300 nM (Fig. S6). Washed platelets were incubated with RWJ-53308 at 0.100, 0.316, 1.00, 3.16, 10.0, and 31.6 μM for 5 min before addition of **1a** or collagen (EC_{60-70}). Three samples of **1a** were used with different incubation periods (15 min, 45 min, and 2 weeks). The potency of the antagonist was greater at the shorter incubation times.

1. Morris VJ, Gunning AP, Kirby AR (1999) *Atomic Force Microscopy for Biologists* (Imperial College Press, London).
2. Sheiko SS, Moeller M (2007) Atomic force microscopy of polymers: imaging, probing and lithography, In *Macromolecular Engineering, Vol. 3*: *Structure-Property Correlation and Characterization Techniques*, eds Matyaszewski K, Gnanou Y, Leibler L (Wiley, Weinheim), Chap 4, pp 1515–1574.
3. Zhong O, Inniss D, Kjoller K, Ellings V (1993) Fractured polymer/silica fiber surface studied by tapping mode atomic force microscopy. *Surface Sci* 290:L688.
4 Magonov SN, Elings V, Whangbo M-H (1997) Phase imaging and stiffness in tapping-mode atomic force microscopy. *Surface Sci* 372:L385.
5. Tamayo J, Garcia R (1997) Effects of elastic and inelastic interactions on phase contrast images in tapping-mode scanning force microscopy. *Appl Phys Lett* 71:2394.
6. Tamayo J, Garcia R (1998) Relationship between phase shift and energy dissipation in tapping-mode scanning force microscopy. *Appl Phys Lett* 73:2926.
7. Garcia R, Tamayo J, Paolo A (1999) Phase contrast and surface energy hysteresis in tapping mode scanning force microscopy. *Surface Interface Anal* 27:312.
8. Cleveland JP, Anczykowski B, Schmid AE, Elings VB (1998) Energy dissipation in tapping-mode atomic force microscopy. *Appl Phys Lett* 72:2613.
9. Scott WW, Bhushan B (2003) Use of phase imaging in atomic force microscopy for measurement of viscoelastic contrast in polymer nanocomposites and molecularly thick lubricant films. *Ultramicroscopy* 97:151.
10. Hoekstra WJ, *et al.* (1999) Potent, orally active GPIIb/IIIa antagonists containing a nipecotic acid subunit. Structure-activity studies leading to the discovery of RWJ-53308. *J Med Chem* 42:5254–5265.

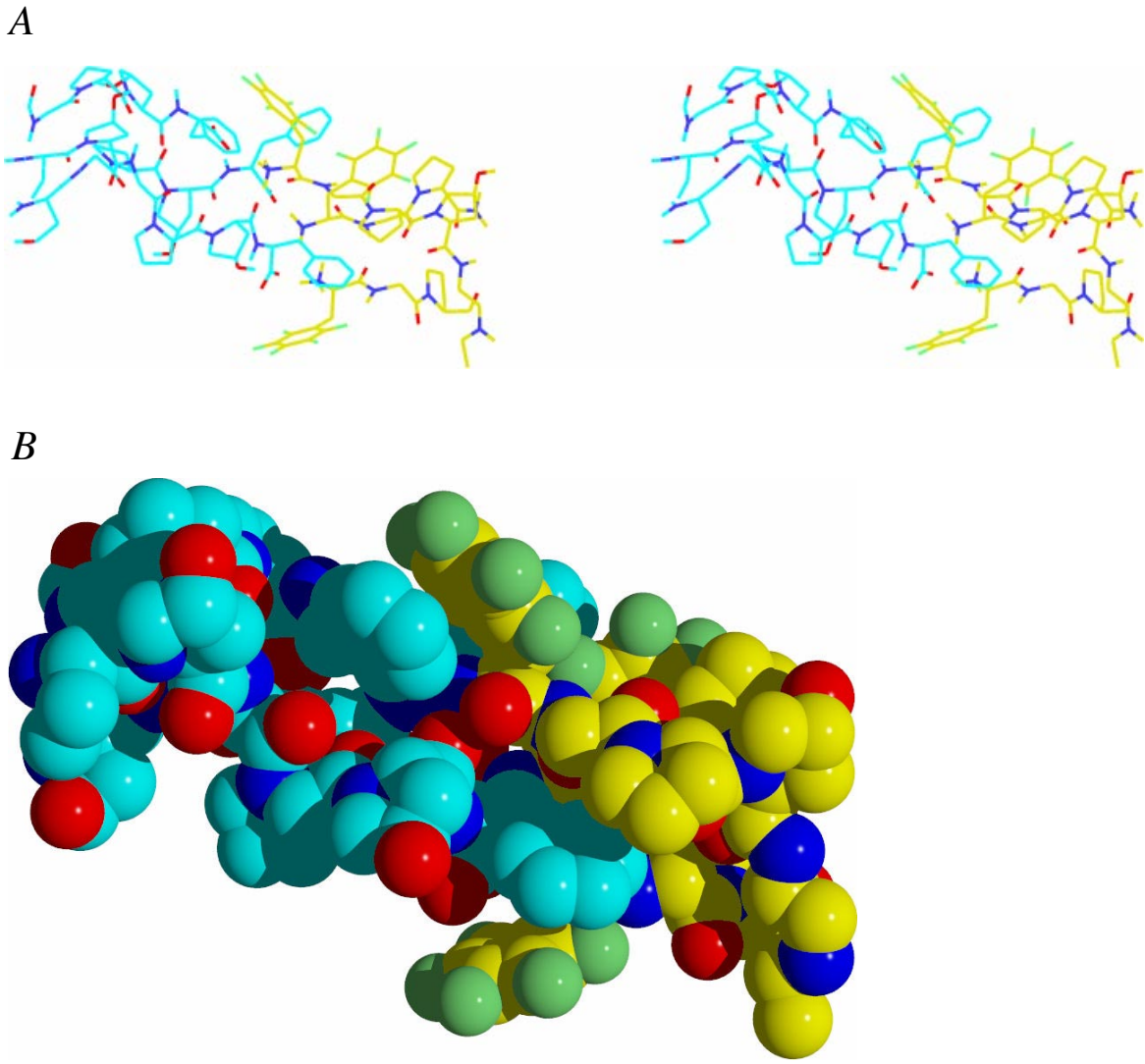

Fig. S1. Additional representations of the head-to-tail interface from the energy-minimized structure of triple-helical, homodimer (**1a**′)$_3$/(**1a**′)$_3$, shown in Fig. 2. (*A*) Relaxed-eye stereoview of the interface. (*B*) Space-filling model of the interface to depict the close packing of aromatic rings and their shielding of the ammonium groups.

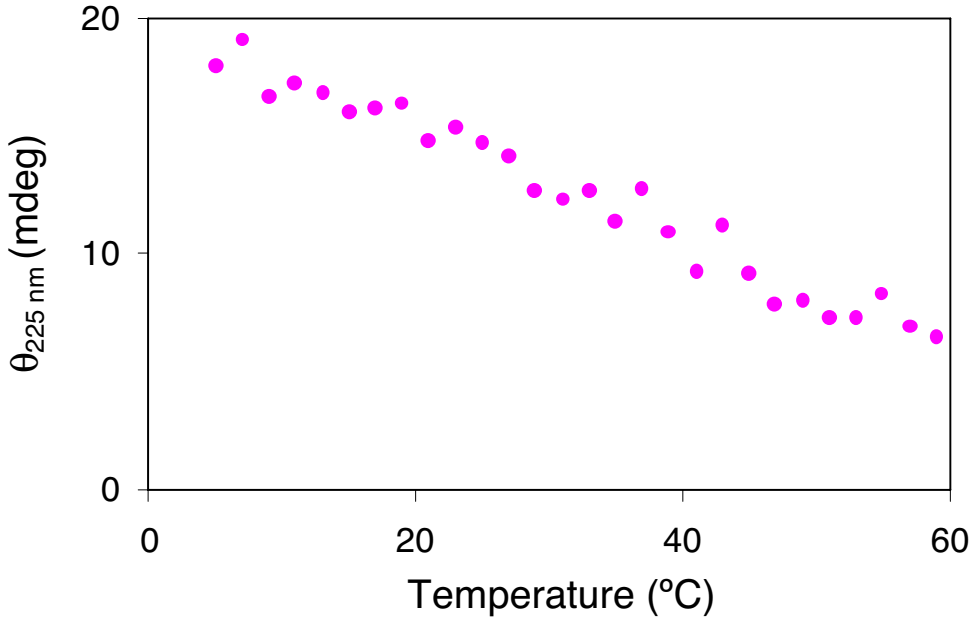

Fig. S2. CD melting experiment for peptide **2**.

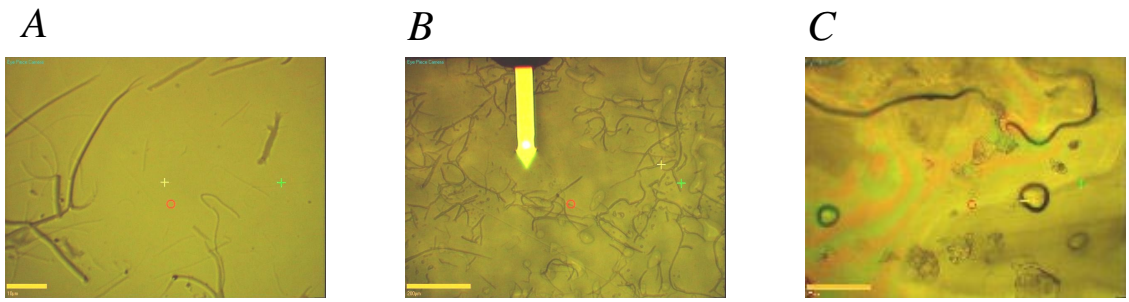

Fig. S3. Light microscopy images of **1a**, **1d**, and collagen. (*A*) Fibrils formed from **1a**. (*B*) Equine type-I collagen fibrils at higher magnification. (*C*) Absence of fibrils with **1d**. (Scale bars: *A*, 10; *B*, 200; and *C*, 80 μm.)

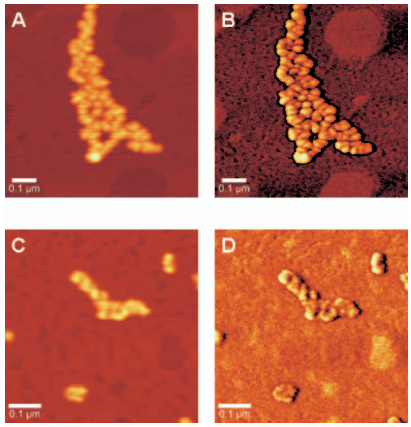

Fig. S4. High-resolution AC-AFM images of **1a** and **1b** adsorbed on freshly cleaved mica. Shown are topography (*A*) and phase (*B*) images of **1a** and topography (*C*) and phase (*D*) images of **1b**. Axial cross-section measurements across three subunits yielded a periodicity pattern, *D*, of ≈33 ± 3 nm for **1a** and **1b**. (Scale bars: 0.1 μm.)

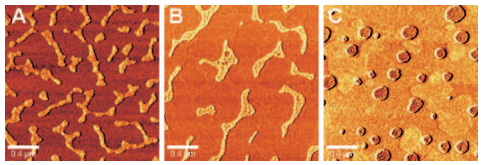

Fig. S5. AC-AFM phase images of **1a** (*A*), **1b** (*B*), and **1c** (*C*). The lighter intensity regions correspond to stiffer material. (Scale bars: 0.4 μm.)

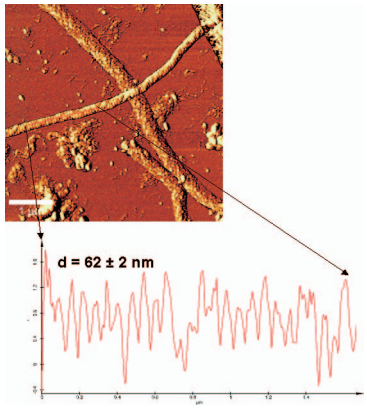

Fig. S6. AC-AFM topography image of equine type-I collagen adsorbed on freshly cleaved mica with an axial cross-section measurement indicating a periodic band gap of 62 nm. (Scale bars: 1 μm.)

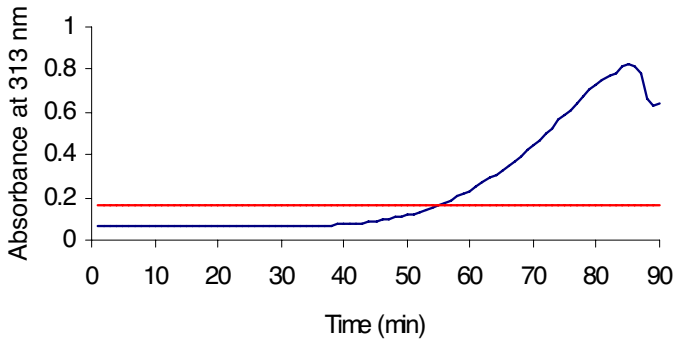

Fig. S7. Turbidity experiments. Absorbance at 313 nm vs. time for **4** (blue) and **1a** (red).

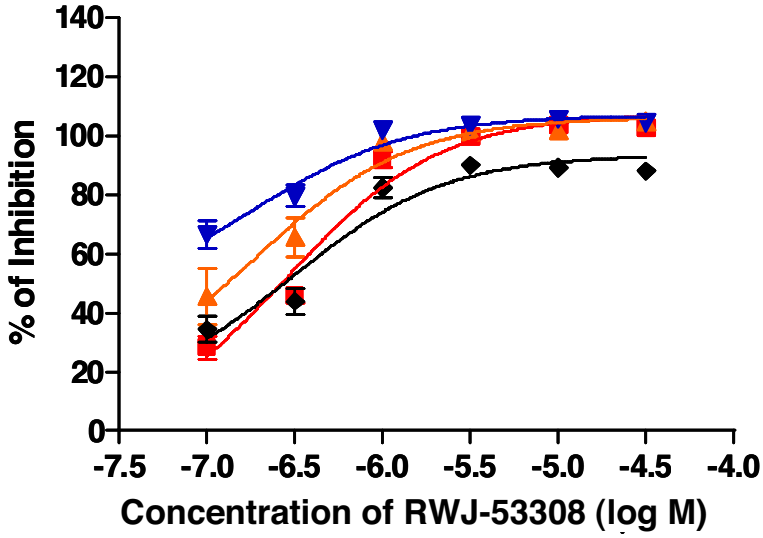

Fig. S8. Inhibition of collagen-stimulated (red) or **1a**-stimulated platelet aggregation by varying molar concentrations of GPIIb/IIIa antagonist RWJ-53308. Solutions of **1a** were prepared in PBS and aged for different times before stimulation of the platelets (15 min, orange; 45 min, blue; 2 weeks, black).

Table 1. Full minimization results for triplex homodimers of 29-mer peptides 1a′–1d′.

Dimer of	XED force field minimized energy, kcal/mol	RMS exit limit, kcal/mol/Å	Total binding energy, kcal/mol	Coulombic binding energy, kcal/mol	Dispersive binding energy, kcal/mol
1a′	4,028.3	0.009	−83.5	−27.7	−55.8
1b′	3,924.6	0.009	−70.4	−16.8	−53.6
1c′	3,894.0	0.009	−58.9	−16.3	−42.6
1d′	3,852.4	0.010	−43.8	−22.2	−21.6

Table 2. Platelet aggregation EC_{50} values (±SEM)

Agent	EC_{50}, μg/ml
Collagen	0.41 ± 0.08
1a*	4.1 ± 0.5
1b*	8.6 ± 0.9
1c*	>30
1d*	>30

*Incubated at 4°C for 7 days.

Table 3. Platelet aggregation EC_{50} values (±SEM)

Agent	EC_{50}, μg/ml
Collagen	0.63 ± 0.06
1a*	2.0 ± 0.4
1b*	2.1 ± 0.3
4*	>30
1a†**	1.1 ± 0.1
1b†**	1.6 ± 0.3
2†**	>30
4†**	>30

*Incubated at 37°C for 80 min.
†Incubated at 4°C for 7 days.

Table 4. Analysis of peptides 1a–1d and 2.

CMP	MS formula	Calculated MS, Da	Found MS, Da*	Yield, %	Peptide content, %†
1a	$C_{138}H_{185}F_5N_{32}O_{43}$ + Na	3,096.3	3096.7	31	73
1b	$C_{138}H_{190}N_{32}O_{43}$ + Na	3,006.4	3007.0	26	71
1c	$C_{135}H_{192}N_{32}O_{43}$ + Na	2,972.4	2973.0	35	77
1d	$C_{124}H_{178}N_{32}O_{43}$ + Na	2,826.3	2826.9	32	77
2	$C_{78}H_{100}F_5N_{17}O_{23}$ + H	1,738.7	1738.7	46	61

*Molecular mass for MS formula from MALDI-TOF MS.
†Accounting for CF_3CO_2H, water, and any residual solvents.